

PAPER

On the PZT/Si unimorph cantilever design for the signal-to-noise ratio enhancement of piezoelectric MEMS microphone

To cite this article: Yu-Chen Chen *et al* 2021 *J. Micromech. Microeng.* **31** 105003

View the [article online](#) for updates and enhancements.



ECS The Electrochemical Society
Advancing solid state & electrochemical science & technology
2021 Virtual Education

Intensive Short Courses

Sunday, October 10 & Monday, October 11

Providing students and professionals with in-depth education on a wide range of topics

[CLICK HERE TO REGISTER](#)



On the PZT/Si unimorph cantilever design for the signal-to-noise ratio enhancement of piezoelectric MEMS microphone

Yu-Chen Chen¹, Sung-Cheng Lo², ShaoDa Wang², Yi-Jia Wang², Mingching Wu³ and Weileun Fang^{1,2,*} 

¹ Institute of Nano Engineering and MicroSystem, National Tsing Hua University, Hsinchu, Taiwan

² Power Mechanical Engineering, National Tsing Hua University, Hsinchu, Taiwan

³ Coretronic MEMS Corp., Hsinchu, Taiwan

E-mail: fang@pme.nthu.edu.tw

Received 1 June 2021, revised 5 August 2021

Accepted for publication 18 August 2021

Published 2 September 2021



Abstract

This study presents the design, fabrication, and testing of a novel piezoelectric micro-electro-mechanical-systems microphone with the partially removed lead zirconate titanate (PZT) unimorph structure for signal-to-noise ratio (SNR) enhancement. To demonstrate the feasibility of the presented concept, the unimorph cantilever array with the patterned (triangular shape) PZT film on top of a rectangular Si layer is simulated, fabricated, and tested. In comparison, the rectangular and triangular unimorph cantilever arrays with fully covered PZT film are also investigated. The proposed and reference cantilever arrays have the same foot print for fair comparison. Simulations show the proposed design has the highest output electrical energy which indicates the proposed design could successfully enhance the SNR. Moreover, acoustic measurements in the standard anechoic box show the proposed Si cantilever with patterned PZT film design could significantly improve the SNR. As compared to the reference microphone with triangular PZT/Si unimorph cantilever, the proposed design shows a 9.8 dB enhancement in SNR. Finally, the influences of initial structure deflections (due to the thin film residual stresses) on the low frequency responses for proposed and reference microphone designs are also investigated.

Keywords: piezoelectric microphone, unimorph structure, cantilever array, PZT, SNR

(Some figures may appear in color only in the online journal)

1. Introduction

The micro-electro-mechanical-systems (MEMS) microphones have been widely used in electronic products, especially in consumer applications. As compared with the traditional electret condenser microphone, the MEMS microphones have the advantages of small size and have the

ability to tolerate high temperature in solder reflow process. Moreover, due to the characteristics of batch fabrication for micromachining, the cost of MEMS microphones can be reduced. In recent years, voice-control has gradually become an important human-machine communication interface. In addition to smartphones, the voice input technology has found various new applications such as wearables, smart homes, automobiles, and so on. Thus, the demand for MEMS microphones will continue to increase, and the speech recognition

* Author to whom any correspondence should be addressed.

will become a concern for MEMS microphones. Some features like beam-forming or directional sound-capturing even require multiple MEMS microphones to form an array [1, 2]. All these factors have boosted the demands for high quality and quantity of MEMS microphones.

The capacitive sensing mechanism has been extensively used in the commercial MEMS microphones [3]. Generally, the capacitive MEMS microphone consists of gap-closing sensing electrodes (including the deformable/movable electrode and the fixed reference electrode). Thus, the air damping effect is a design concern for the gap-closing electrode. The design of capacitive sensing electrodes trades off between the sensing area and the vent-hole area (to reduce air damping) [3–8]. Also, the small air gap for capacitive sensing is very vulnerable to water and dust particles. This is a critical design concern for the growing microphone array applications since the damage of a single microphone may cause the entire array lose its function. In addition to the capacitive sensing MEMS microphone, the piezoelectric counterpart has attracted attentions in recent years. The back plate and sensing gap are not required for the piezoelectric microphones [9, 10]. Hence, the air damping due to the small sensing gap is not a design concern and the structure is less sensitive to the water and dust. Moreover, the piezoelectric microphone could offer large dynamic range [11] and low power consumption to enable it a promising solution for wide applications. The simple transduction mechanism of piezoelectric sensing has also been adopted to realize unconventional microphone designs such as the broadband microphone imitating the structure of human cochlea [12], and the directional microphone inspired by insect organ [13, 14]. Nevertheless, the signal-to-noise ratio (SNR) of piezoelectric microphone is still lower than that of the capacitive counterpart. The enhancement of SNR is an important design concern for the piezoelectric microphone.

As discussed in [15–17], to increase the output electrical energy of the piezoelectric microphone would be a general design guideline to reduce its noise floor. Thus, piezoelectric microphones of different structures but the same volume of back cavity are investigated accordingly. Moreover, the piezoelectric microphone with the characteristic of $SNR^2 \propto$ output electrical energy is also presented in [18]. In most of the studies, cantilever is adopted as the structure of the piezoelectric microphone, since it has the highest mechanical sensitivity comparing with bridge or clamped diaphragm structures [19]. By following the terminologies extensively used in piezoelectric MEMS transducers [20], the MEMS structure with the stacking of single piezoelectric layer and other thin films named ‘unimorph structure,’ and the MEMS structure with the stacking of two piezoelectric layers and other thin films named ‘bimorph structure’. This study mainly focuses on the investigation of unimorph cantilever. Most of the existing unimorph cantilevers are fully covered with the piezoelectric layer [19, 21]. Nevertheless, unimorph cantilevers with the patterned piezoelectric layer are presented in [9, 22–24]. In these studies, the piezoelectric layer is distributed near the anchor of the cantilever, yet no design issues are discussed. The piezoelectric layer can be a critical design parameter to influence the stiffness and stress distribution of unimorph cantilever,

and also the charges generated after applying external loads. This study extends the designs in previous work [25] to present the piezoelectric microphone which consists of a cantilever structure with partially removed lead zirconate titanate (PZT) layer. Based on the proposed design, the output electrical energy of the device is increased and the SNR is improved.

2. Design concepts and principles

The working principle of the proposed piezoelectric microphone is illustrated in figure 1. The microphone consists of the cantilever diaphragms formed by the Si and PZT unimorph structure. (The top and bottom electrodes are neglected in this illustration.) As shown in figure 1(a), an in-plane bending stress $\Delta\sigma$ will be introduced on the cantilever when a sound pressure ΔP is applied. Under the condition of small piezoelectric coupling (SPC) assumption [15] (measurements in section 4.1 will show the reasonable assumption of SPC), the effect of the electric field can be ignored, and the inverse-piezoelectric effect is not considered. Thus, the piezoelectric sensing mechanism could be simplified as,

$$D = d_{31}\Delta\sigma \quad (1)$$

$$\Delta Q = \int D dA \quad (2)$$

where D is the electric displacement, d_{31} is the transverse piezoelectric coefficient, ΔQ is the charge signal, and A is the electrode area. Figure 1(b) summarizes the sensing schema of the proposed piezoelectric MEMS microphone. To enhance the signal, this study will be mainly focus on the mechanical transduction (the first transduction in figure 1(b)), which is to increase the bending stress induced by the sound pressure.

Based on the Euler–Bernoulli bending theory, as a bending moment M applied on a beam, the normal stress σ distributed in the beam can be expressed as [26],

$$\sigma = \frac{My}{I} \quad (3)$$

where y is the distance from the neutral axis to a point of interest; and I is the moment of inertia of the cross-sectional area with respect to its centroidal axis. Figure 2(a) displays a typical rectangular composite (unimorph) beam consisted of a micromachined Si cantilever of thickness h_c and a PZT film of thickness h_p . In this case, the planar dimensions (length and width) of the Si cantilever and the PZT film are identical. According to [26], the location of neutral axis is determined by the cross-section area and young’s modulus of Si (A_{Si} and E_{Si}) and PZT film (A_P and E_P). Moreover, the distance y_{max} ($y_{max} = y_1$ in this case) from the neutral axis to the top surface of the PZT film is also varying with A_{Si} , E_{Si} , A_P and E_P . For given materials (Si and PZT film) of the composite beam, this study proposed the unimorph cantilever with patterned PZT film as depicted in figure 2(b) to decrease the cross-section area of A_P by partially removing the PZT film. Thus, the neutral axis of the composite beam will shift downward to increase the distance y_{max} (in this case $y_{max} = y_2$, and $y_2 > y_1$), and then

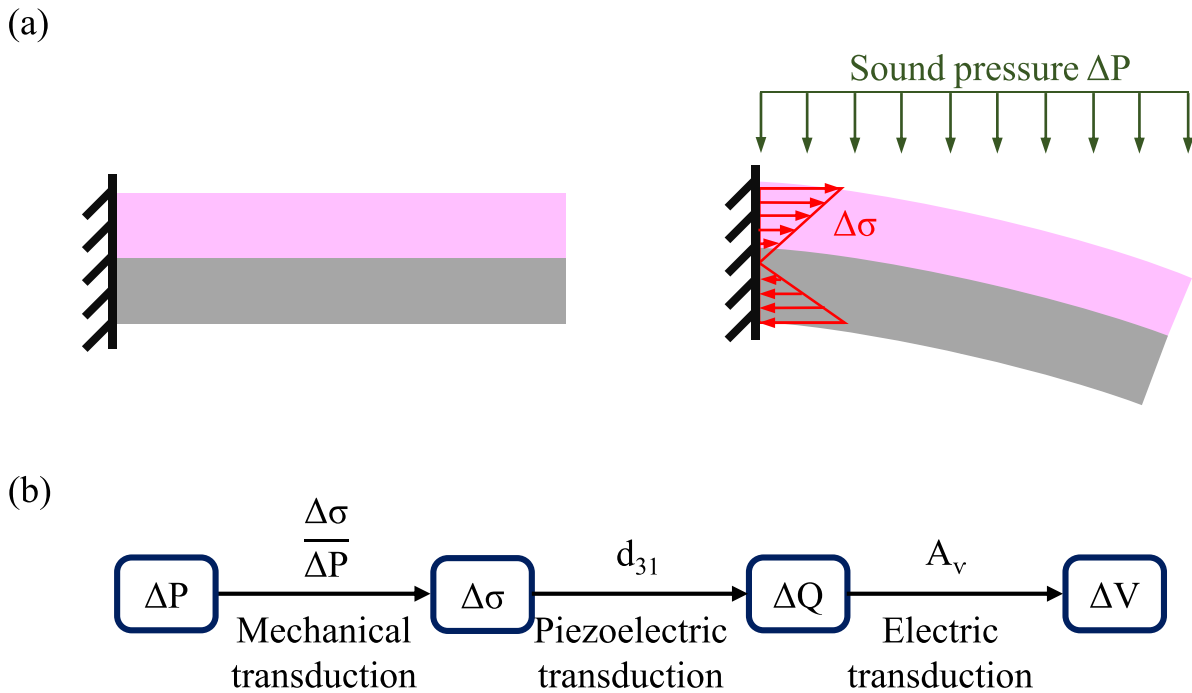


Figure 1. (a) Schematic diagram of the unimorph cantilever consisted of the Si and PZT layers and (b) working principle of the proposed piezoelectric MEMS microphone.

the bending stress introduced on the PZT film is increased. In addition, the net moment of inertia I of the composite beam will also drop after the decrease of A_p . Note that the proposed (in figure 2(b)) and reference (in figure 2(a)) designs have the same area to receive the sound pressure (i.e. the rectangular Si cantilever), and hence the bending moments M applied on these two cantilevers are the same. Thus, as depicted in equation (3), the bending stress of the proposed design could be effectively increased since it could increase the y_{max} and also decrease the I . The schematic illustration with all layer stacking is shown in the side-view of figure 2(c).

This study further presents the microphone devices consisted of the PZT/Si unimorph cantilever array to demonstrate the feasibility of the proposed concept. The microphone devices will be fabricated on the silicon on insulator(SOI) wafer with PZT layer as the piezoelectric film, and hence the unimorph cantilever is consisted of the Si and PZT layers. The schematic illustrations in figure 3 display three different microphone designs (with unimorph cantilever array) investigated in this study. Each microphone is composed of four PZT/Si unimorph cantilevers suspended on a back cavity. The proposed unimorph cantilever design with the patterned PZT film on top of a rectangular Si is shown in figure 3(a). Note that this study employs the triangular shape as the preliminary design for the PZT film. Nevertheless, the shape of the PZT film can still be optimized for future applications. Figures 3(b) and (c) depict two reference designs for comparison. Figure 3(b) shows the reference design with un-patterned PZT film. The reference one in figure 3(c) follows the triangular piezoelectric cantilever design of the commercial microphone in [27]. For fair comparison, all of the microphones have the same die size (1.5 mm × 1.5 mm) and the diaphragm area (800 μm × 800 μm).

The mechanical responses of the proposed and reference designs under 1 Pa 1 kHz sound pressure load are simulated using the commercial finite element method (FEM) software (COMSOL). As the FEM simulation shown in figure 4(a), for the proposed rectangular Si cantilever with triangular PZT layer, the average normal stress (in-plane direction) on top surface of PZT film is 13.0 kPa. While in figure 4(b), the reference design with rectangular PZT/Si composite cantilever will reduce the average normal stress on top surface of PZT film to 10.4 kPa. As depicted in figure 4(c), the reference triangular PZT/Si unimorph cantilever design will further reduce the average normal stress on top surface of PZT film to only 3.7 kPa. Simulation results show that with the same input sound pressure, the proposed unimorph cantilever design with rectangular Si and triangular PZT layers can increase the stress for up to 25% as compared to the rectangular PZT/Si unimorph cantilever and up to 251% when comparing to the triangular PZT/Si unimorph cantilever.

This study employs the commercial multiphysics FEM software to predict the performance of piezoelectric microphones. According to [14–17], simulations mainly focus on the output electrical energy of the proposed and reference piezoelectric microphones (in figure 2) with different length percentage of top electrode coverage. Schematic illustration of ‘the length percentage of top electrode coverage’ is depicted in figure 5(a). In short, the ‘length percentage of 0%’ is defined at the anchor of the cantilever and the ‘length percentage of 100%’ is defined at the tip of the cantilever. Simulation results in figure 5(b) depict the output electrical energy of the proposed and reference unimorph cantilever designs varying with ‘the top electrode coverage percentage’. The variation of output electrical energy with the length percentage of top electrode coverage is resulted from the stress distribution on

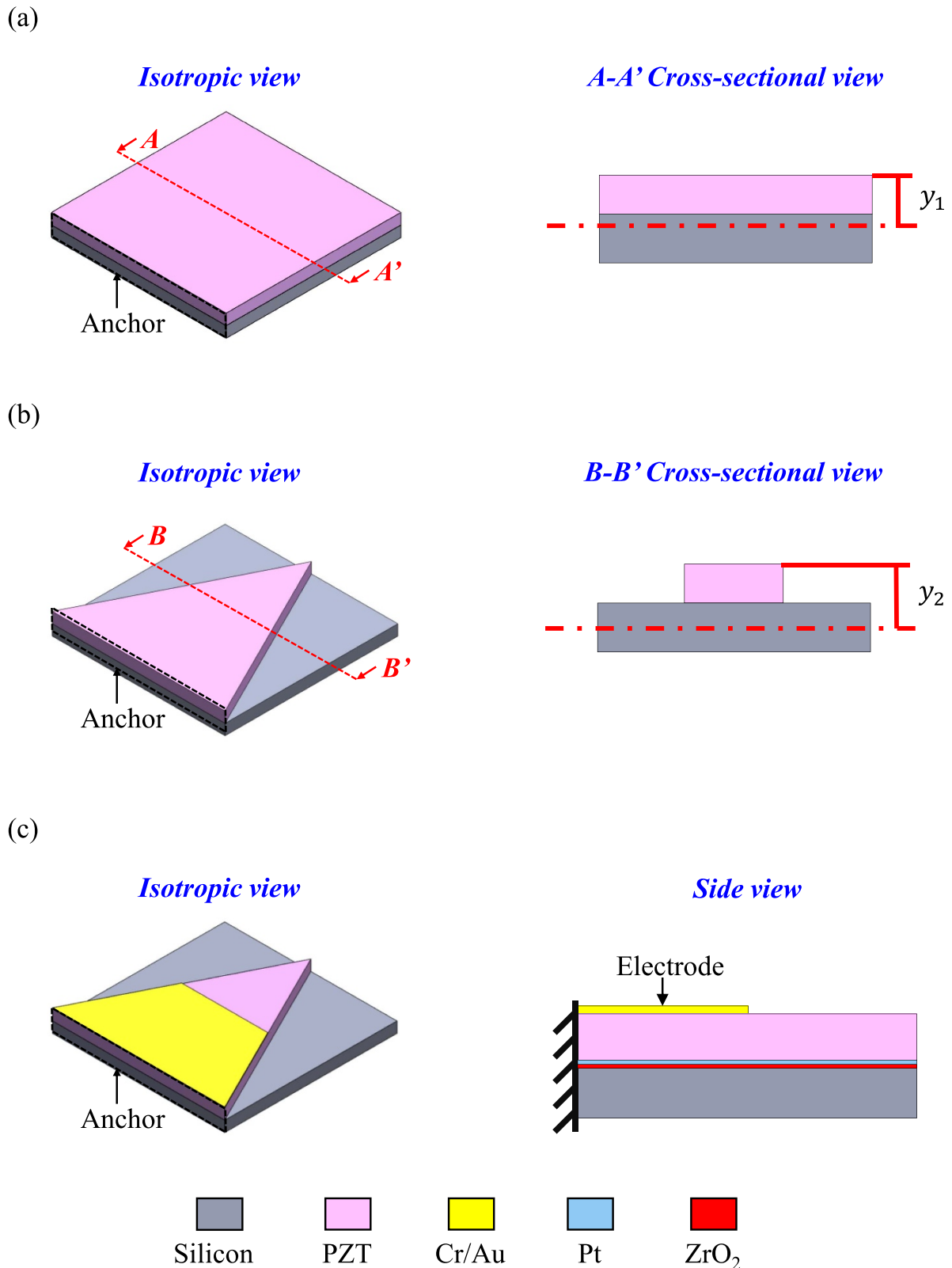
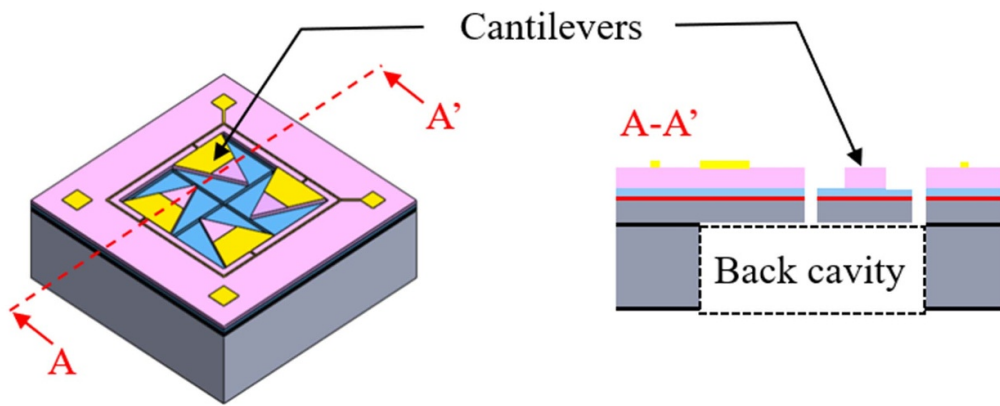


Figure 2. (a) The rectangular Si cantilever fully covered with the PZT film, (b) the rectangular Si cantilever covered with the patterned PZT film and (c) the rectangular Si cantilever with the patterned PZT film and top electrode.

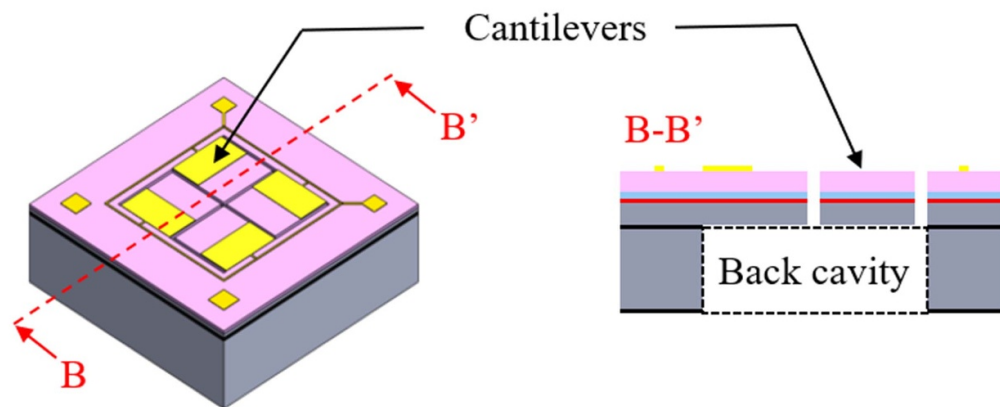
cantilever and the initial capacitance on electrodes. As shown in figure 4, the largest stress is distributed at the fixed-end of cantilever yet relatively small stresses are distributed near the free-end of beam. In this regard, for the 100% coverage

condition, the electrodes covered near the free-end of cantilever will mainly contribute the initial capacitance, so that the output energy will be reduced. Therefore, the output energy can be increased if partially remove the electrode near the

(a) Proposed Si rectangular cantilever with patterned PZT film



(b) Reference PZT/Si rectangular cantilever



(c) Reference PZT/Si triangular cantilever

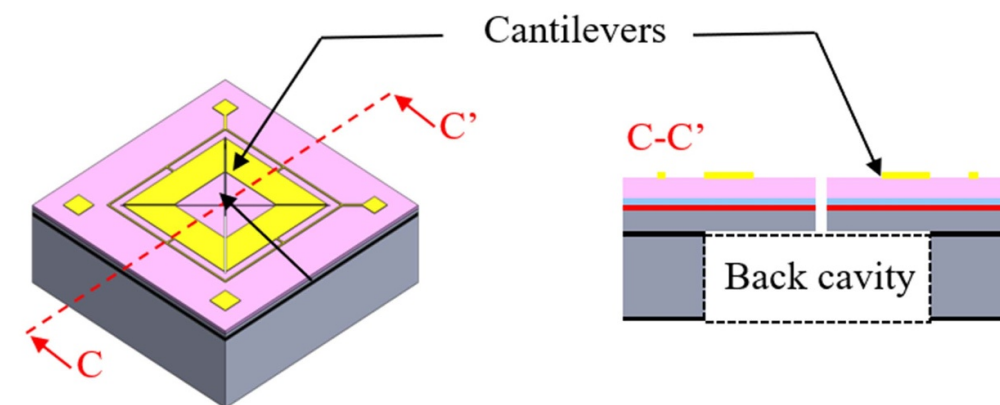


Figure 3. (a) The proposed rectangular Si cantilever with patterned PZT film, (b) the reference PZT/Si rectangular cantilever, and (c) the reference PZT/Si triangular cantilever.

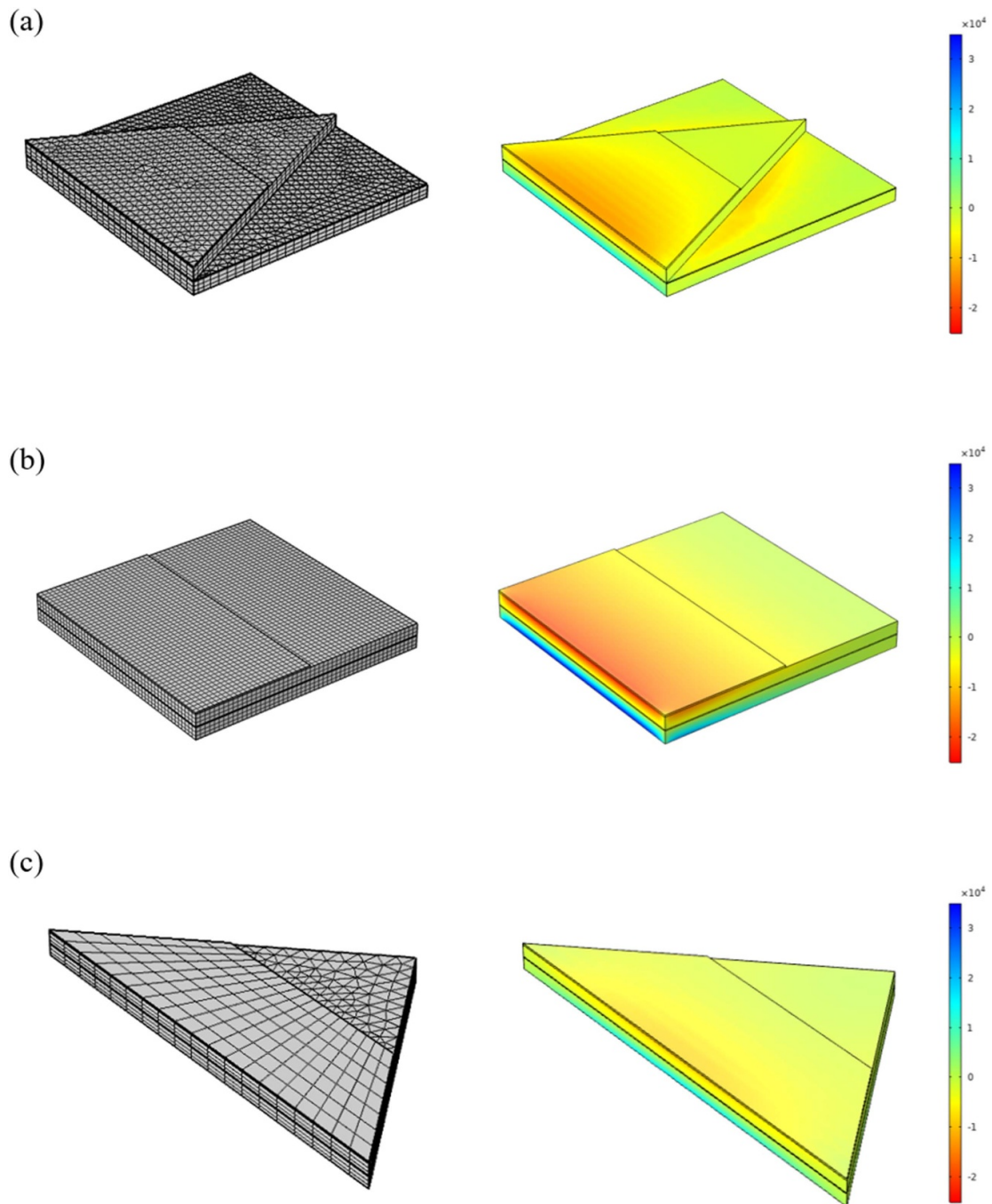


Figure 4. The FEM simulation models and results for, (a) the proposed rectangular Si cantilever with patterned PZT film, (b) the reference PZT/Si rectangular cantilever, and (c) the reference PZT/Si triangular cantilever.

free-end of cantilever. Moreover, the output electrical energies are also different for these three unimorph cantilever designs. The maximum output electrical energy of the proposed rectangular Si cantilever with triangular PZT film design occurs at 50%, whereas the reference designs are respectively at 38% (triangular PZT/Si cantilever) and 42% (rectangular PZT/Si cantilever). The maximum electrical output energy of the proposed design is higher than those of the reference designs. In experiments, this study selects the 50% length percentage of top electrode coverage (indicated in figure 5(b)) as a basis to compare the output electrical energy level of these

three designs. Simulations show that the proposed design has improved the output energy for 522.8% as compared to the reference design with triangle cantilever. It is expected that the rectangular Si cantilever with triangular PZT film unimorph cantilever could improve the SNR ratio. Note that if selecting different ‘length percentage of top electrode coverage’ to have these three designs to respectively reach their maximum output energy, then the output energy enhancement of the proposed design (as compared with the triangle reference design) will be decreased from 522.8% to 504.5%. Thus, the SNR enhancement will be slightly dropped accordingly.

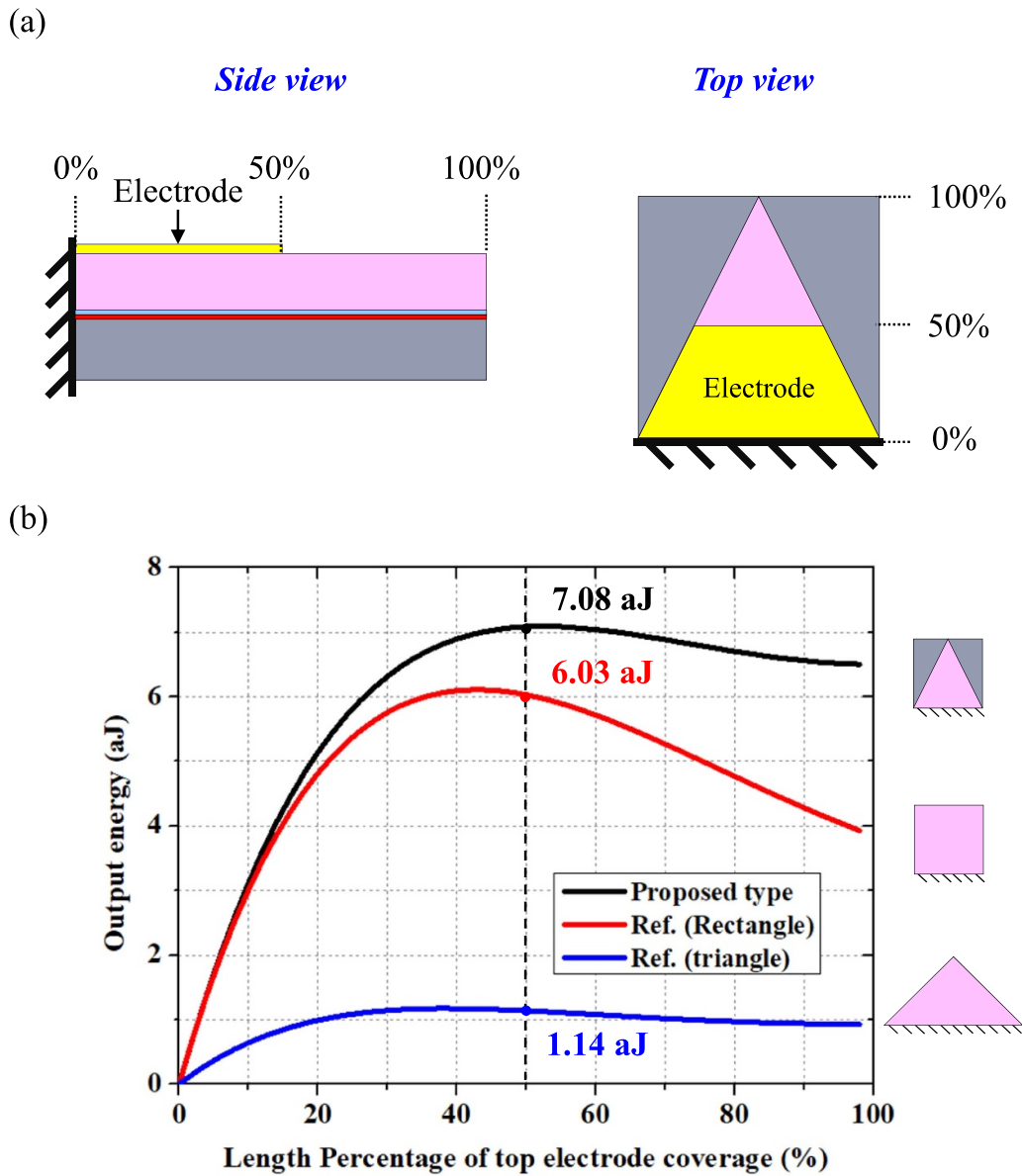


Figure 5. (a) The schematic illustration to show the length percentage of top electrode coverage and (b) the simulated output electrical energies of the proposed and reference unimorph cantilever designs varying with ‘length percentage of the top electrode coverage’.

3. Fabrication and results

The presented microphones were implemented using the fabrication processes shown in figure 6. First of all, an SOI wafer with 2 μm device layer was deposited with a 15 nm thick ZrO₂ and a 150 nm thick Pt thin films. The ZrO₂ layer serves as an insulation layer to prevent current leakage and also an adhesion layer for better Pt adhesion. The Pt layer serves as the bottom electrode. The piezoelectric layer, PZT, was deposited onto the Pt layer by sputtering process. The proposed and reference PZT structure designs were then defined by photolithography and then patterned by the wet etching process as shown in figure 6(a). The bottom electrodes to act as bond pads were exposed simultaneously. As depicted in figure 6(b), the 50 nm thick Cr and the 300 nm thick Au thin films, which serve as the top electrodes and bond pads, were deposited by the electron-beam thermal evaporation and then patterned by the

lift-off process. After that, as shown in figure 6(c), the shapes of the Si cantilevers were defined by the photolithography and then patterned by the front side inductively coupled plasma (ICP) dry etching. In this process, the ICP, which employed the mixed gas (70 sccm of CF₄ and 40 sccm of Ar) and operated under 1 Pa chamber pressure with 800 W RF power and 200 V bias voltage, etched through the PZT, Pt, ZrO₂, Si layers and stopped at the box oxide. As illustrated in figure 6(d), the reactive ion etching (RIE) was used to define the backside thermal oxide. The handle Si layer of the SOI wafer was then etched by deep RIE (DRIE) process, as depicted in figure 6(e). The final step is removing the box oxide by backside RIE to release the cantilevers, as indicated in figure 6(f).

The SEM micrographs in figure 7 display typical fabrication results of the piezoelectric MEMS microphone arrays. The micrograph in figure 7(a) shows the proposed PZT/Si unimorph cantilever design consisted of a rectangular Si layer

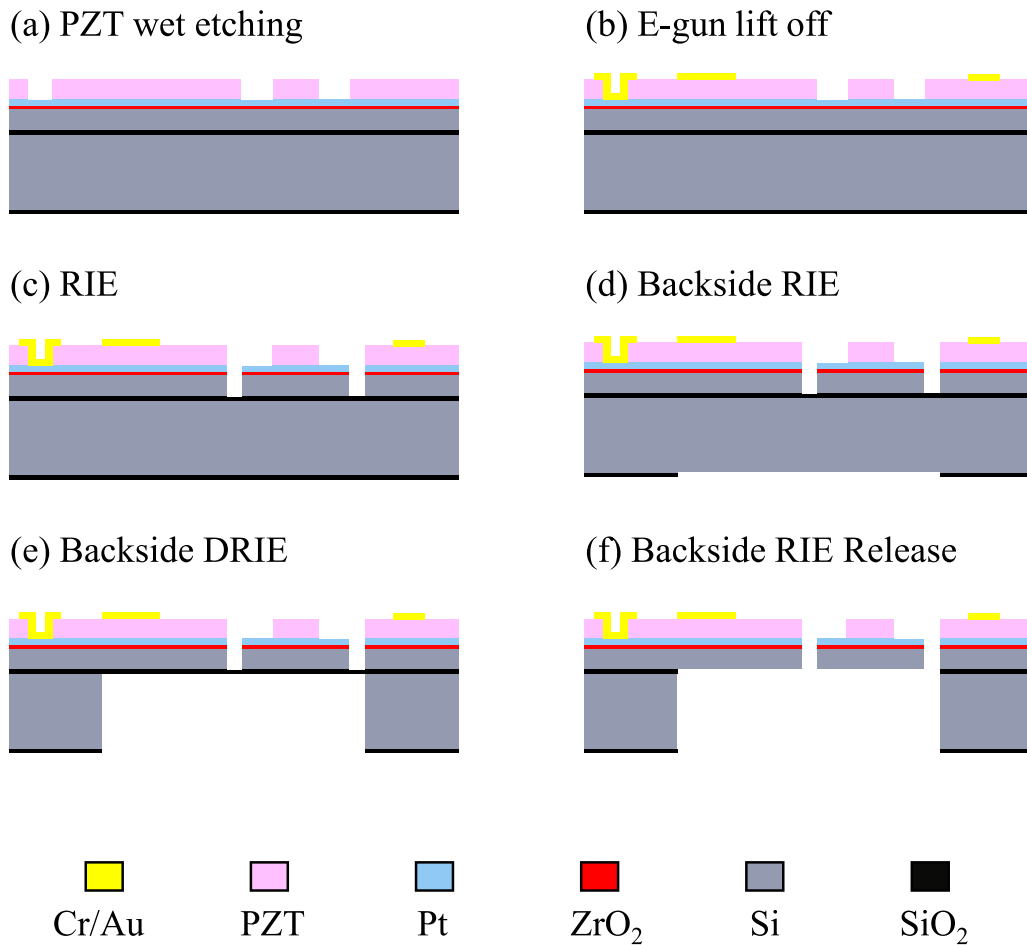


Figure 6. Fabrication process steps.

and a patterned (triangular shape) PZT film. Figure 7(b) displays the reference design which is consisted of the rectangular Si cantilevers fully covered with the PZT layer. Moreover, figure 7(c) exhibits another reference design with triangular Si cantilevers and patterned PZT film. For fair comparison, the proposed and reference PZT microphone arrays in figures 7(a)–(c) have the same footprint of $800\ \mu\text{m} \times 800\ \mu\text{m}$. The micrograph in figure 7(d) displays the back-side cavity of the device defined by the DRIE process on the SOI wafer. The electrode on the cantilever and the electrical routing on the substrate could be observed in the zoom-in micrograph in figure 7(e). In addition, the width of the trenches between cantilevers (and also between the cantilever and the boundary) defined by the process in figure 6(c) could be observed in the same figure. The trench width is around $9.6\ \mu\text{m}$. The cross-section view of the cantilever in figure 7(f) further shows the layer stacking of the unimorph cantilever microphone which consisted of the PZT thin film, the Pt bottom electrode, and the Si device layer.

In this study, the bottom-port packaging approach is adopted for the presented microphones. As shown in figure 8(a), the schematic illustration indicates the overall packaged device. The fabricated MEMS microphone chips are mounted and wire-bonded onto printed circuit boards (PCBs) with a sound inlet hole. Metal cap is grounded and covering above the microphone chip in order to form a back-chamber for acoustic

concern and also to serve as an electromagnetic interference shielding purpose. The volume of the back chamber is $46\ \text{mm}^3$, which is large enough to preclude its influence on the SNR of the microphone [15]. The photo in figure 8(b) show the typical packaged microphone on PCB as the device under testing (DUT). The zoom-in micrographs respectively indicate the presented microphone with metal cap package and the sound inlet hole at the bottom side of PCB. Figures 8(c)–(e) further respectively display the wire-bonded microphone chips of three different designs.

4. Measurement and results

This study has performed experiments to evaluate the material properties of the PZT thin film and the performances of the proposed MEMS microphones. The measured piezoelectric properties of the PZT film and the acoustic performance of the proposed and reference PZT/Si unimorph microphones are presented and discussed in the following subsections.

4.1. Piezoelectric properties of the PZT thin film

The SNR of the proposed piezoelectric microphone is influenced by the material properties of the PZT film. For a given microphone structure and the back chamber volume, the relation between the SNR and the properties of PZT film can be expressed as [18],

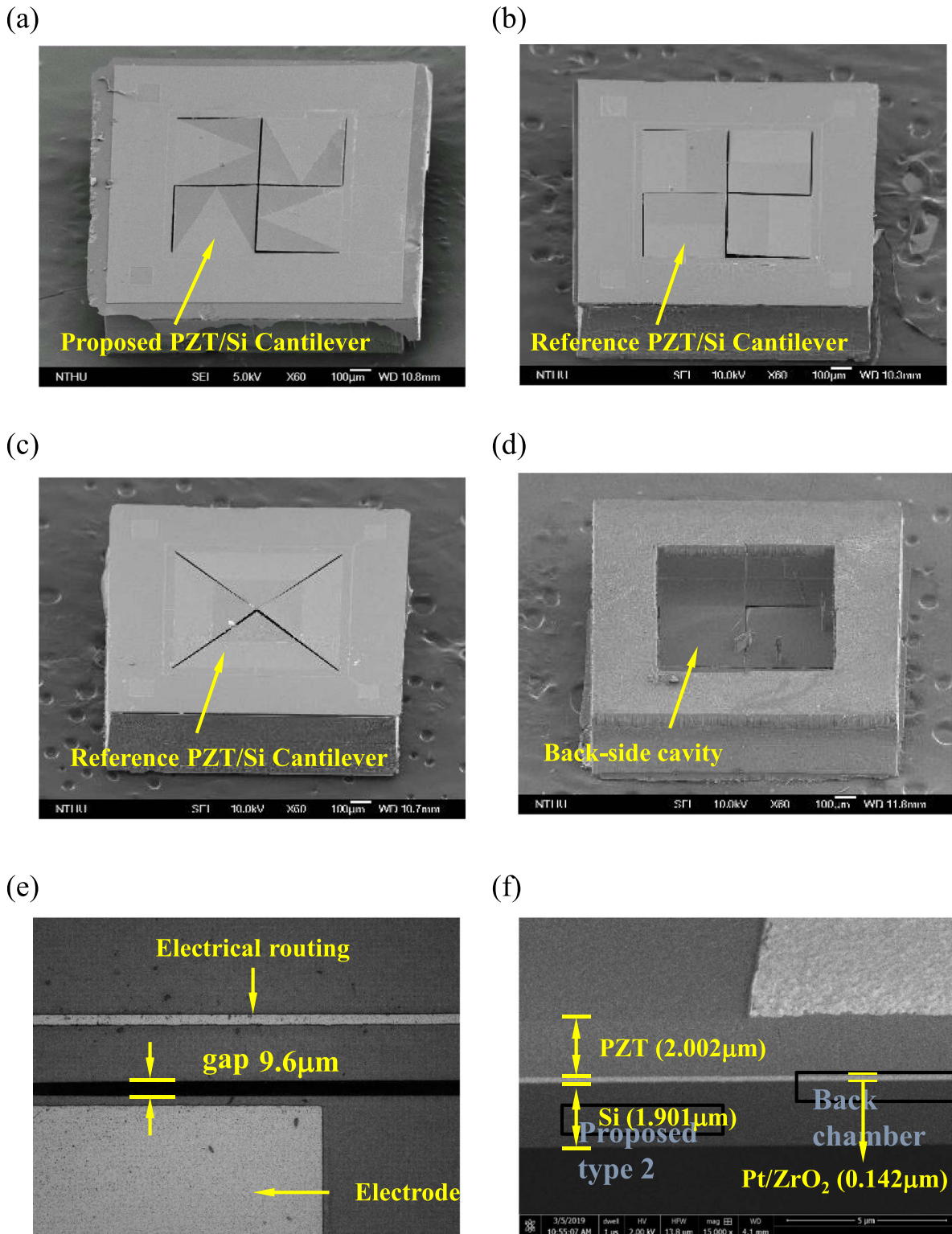
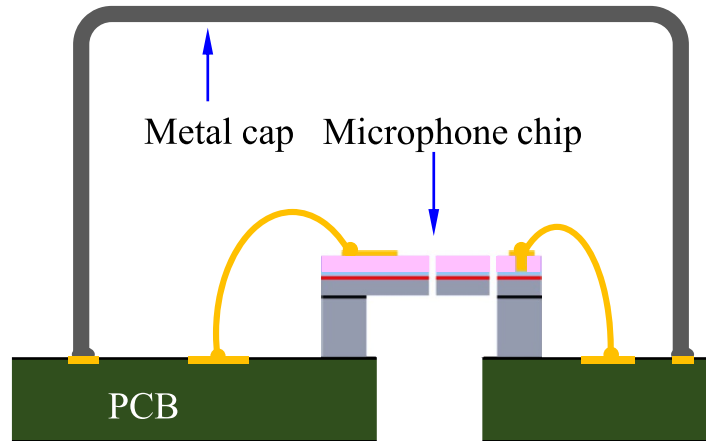
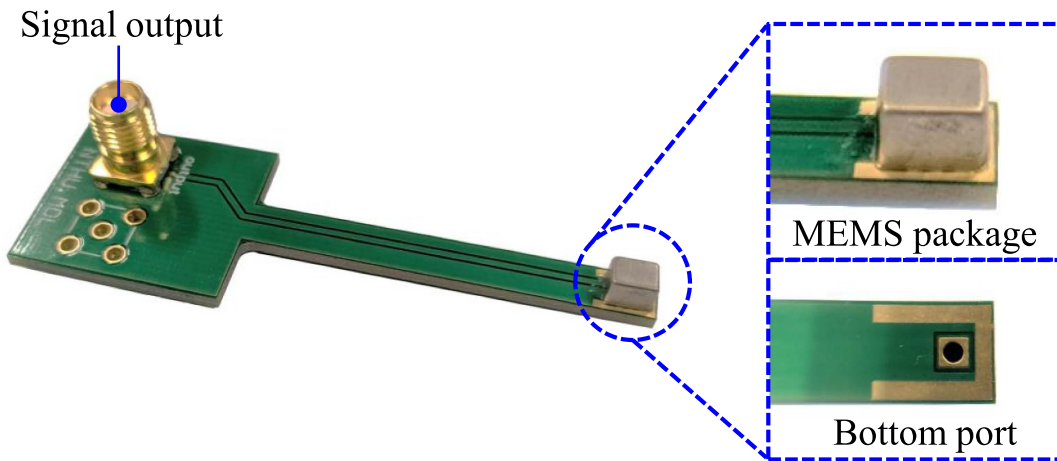


Figure 7. The scanning electron microscope (SEM) micrographs of typical fabricated piezoelectric MEMS microphone arrays, (a) the proposed rectangular Si cantilever with patterned PZT film, (b) the reference PZT/Si rectangular cantilever, (c) the reference PZT/Si triangular cantilever, (d) the back-side cavity of the microphone defined by the DRIE process, (e) the zoom-in micrograph to show the electrode on the cantilever and the electrical routing on the substrate, and the 9.6 μm wide gap surrounded cantilevers is also observed, and (f) the cross-section view of the cantilever to show the layer stacking of the unimorph cantilever including the PZT film, the Pt/ZrO₂ bottom electrode, and the Si device layer.

(a)



(b)



(c)

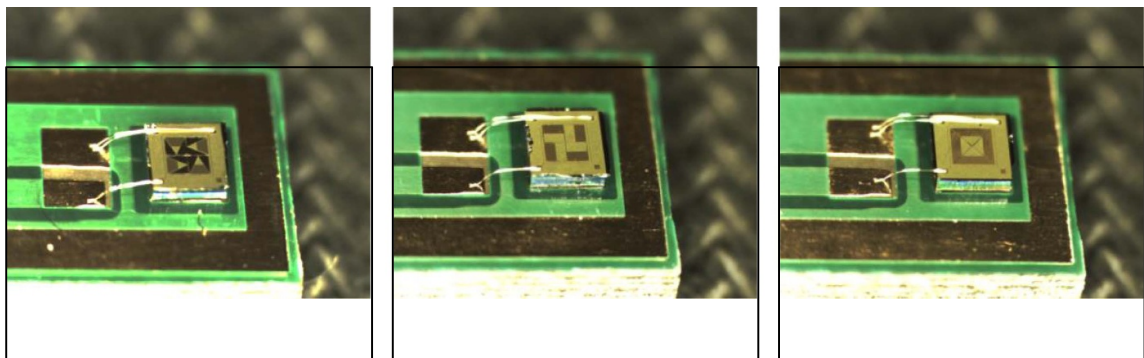


Figure 8. (a) The schematic illustration of the packaged device (microphone chip wire bonded on the PCB and then covered with a metal cap) (b) the photo to show the device under testing, and (c) the micrographs of wire-bonded chips respectively for the proposed and reference designs.

$$\text{SNR}^2 \propto \frac{d_{31}^2}{\epsilon_r \tan \delta} \quad (4)$$

where d_{31} is the piezoelectric coefficient, ϵ_r is the dielectric constant, and $\tan \delta$ is the dielectric loss of the PZT film. The

piezoelectric coefficient d_{31} of the PZT film is determined by the dynamic measurement approach [28, 29]. As shown in figure 9(a), the dynamic displacements (δ_{dy}) and the natural frequencies (ω_n) of the cantilever test keys with different length (250 μm , 300 μm , 400 μm), are measured by the laser

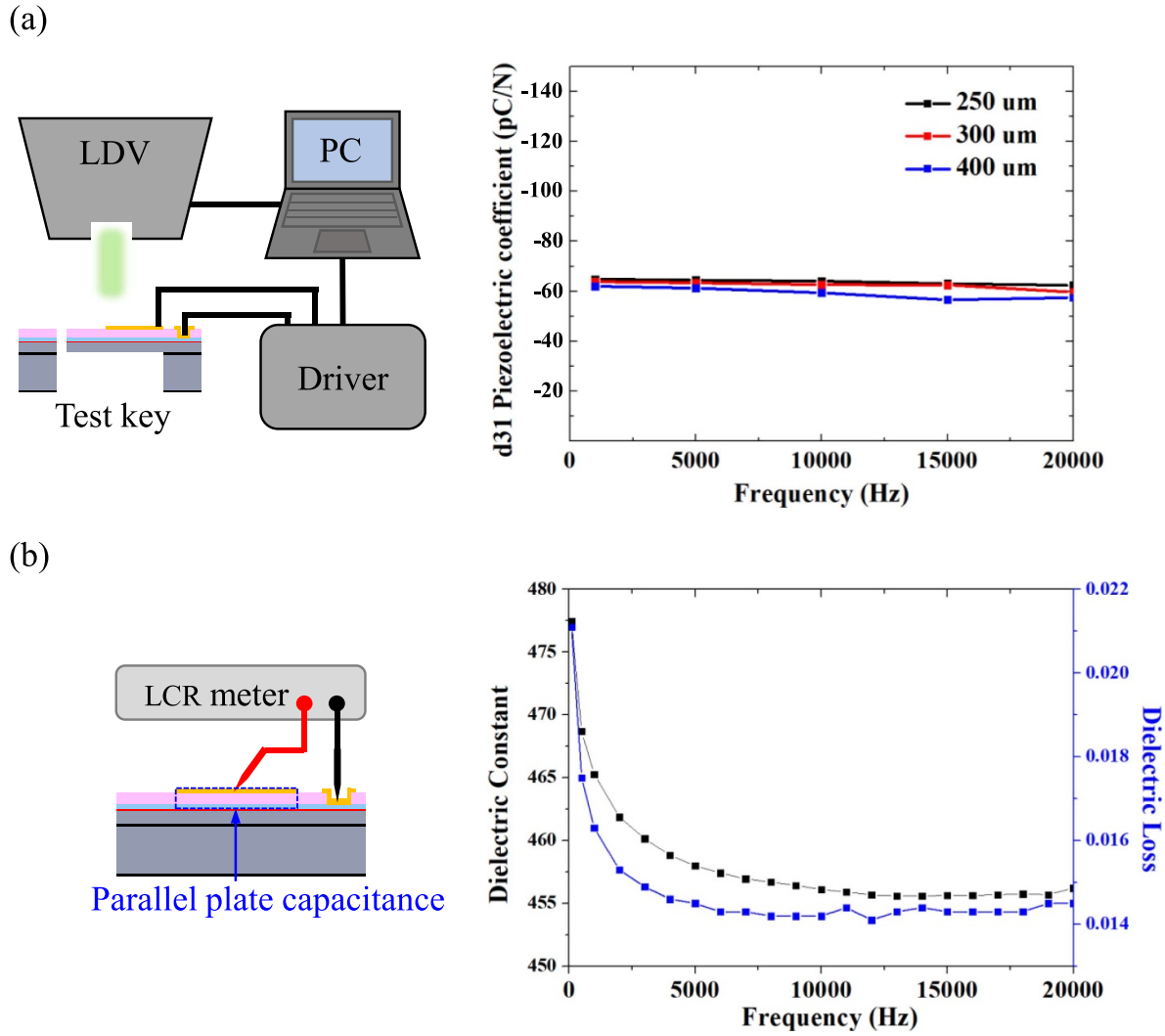


Figure 9. The test setups and results for the measurement of, (a) piezoelectric coefficient (b) dielectric constant.

Doppler vibrometer. The equivalent static displacement δ_{st} can then be determined by the measured dynamic displacement δ_{dy} through [28],

$$\delta_{st} = \sqrt{\left(1 - \left(\frac{\omega_{input}}{\omega_n}\right)^2\right)^2 + \left(2\xi\frac{\omega_{input}}{\omega_n}\right)^2} \times \delta_{dy} \quad (5)$$

where ω_{input} is the driving frequency, ξ is the damping ratio. After that, the d_{31} piezoelectric coefficient could be extracted by [29],

$$\delta_{st} = \frac{3d_{31}s_s s_p t_s (t_s + t_p) L^2 V}{s_s^2 t_p^4 + 4s_s s_p t_s t_p^3 + 6s_s s_p t_s^2 t_p^2 + 4s_s s_p t_s^3 t_p + s_p^2 t_s^4} \quad (6)$$

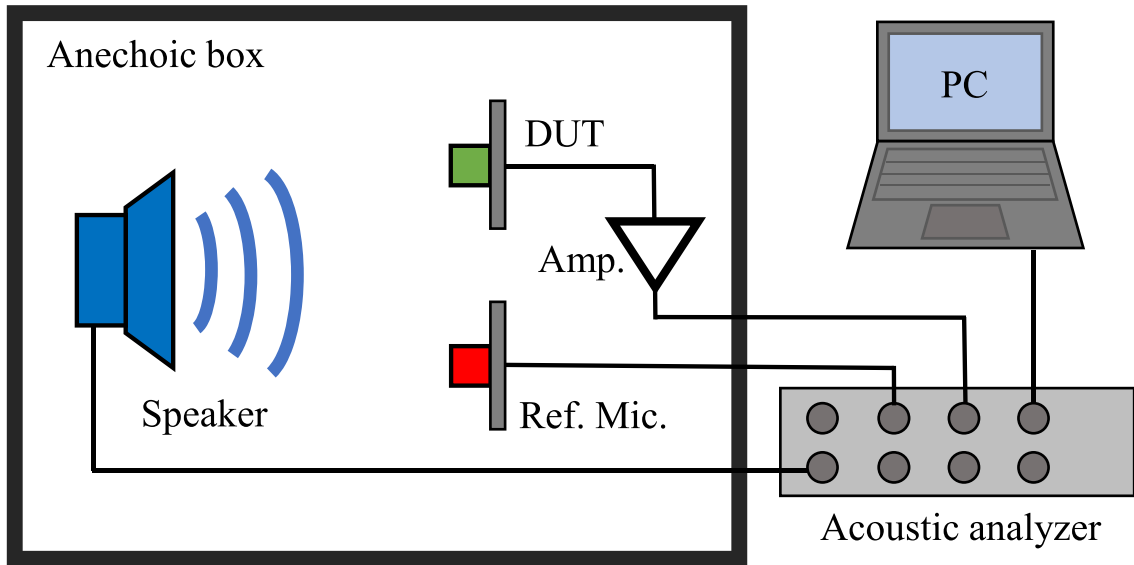
where s_p and s_s are the mechanical compliances of the PZT and Si layer, t_p and t_s are the thickness of the PZT and Si layer, L is the length of the cantilever, and V is the driving voltage. Measurements in figure 9(a) indicate a nearly constant value of d_{31} (-59.5 pC N^{-1}) is observed over the entire bandwidth from 1 kHz to 20 kHz. The dielectric constant and

the dielectric loss of the PZT are measured by directly connecting the parallel plate test key to the LCR meter, as shown in figure 9(b). Measurements show the dielectric constant (at 1 kHz) of PZT is 465.3 and the dielectric loss is 0.0163. Thus, the measured properties of PZT film meet the condition of $d_{31}/\eta_{33}s_{11} \ll 1$ (where η is the electric permittivity matrix and s is the compliance matrix), further showing the assumption of SPC in section 2 is also fulfilled.

4.2. Acoustic performance of the microphone

This study established the setup schematically illustrated in figure 10(a) to test the performances of the presented devices, and the photo of actual layout is shown in figure 10(b). The acoustic performance experiments were conducted in an anechoic box to isolate the ambient noise. Inside the anechoic box, the DUT shown in figure 8(b) and the reference microphone were placed at the same distance from the loudspeaker (KEF Q100). The sound pressure output and the frequency response of the loudspeaker is calibrated by a sound calibrator (GRAS-42 dB, GRAS Sound & Vibration A/S, Denmark) and

(a)



(b)

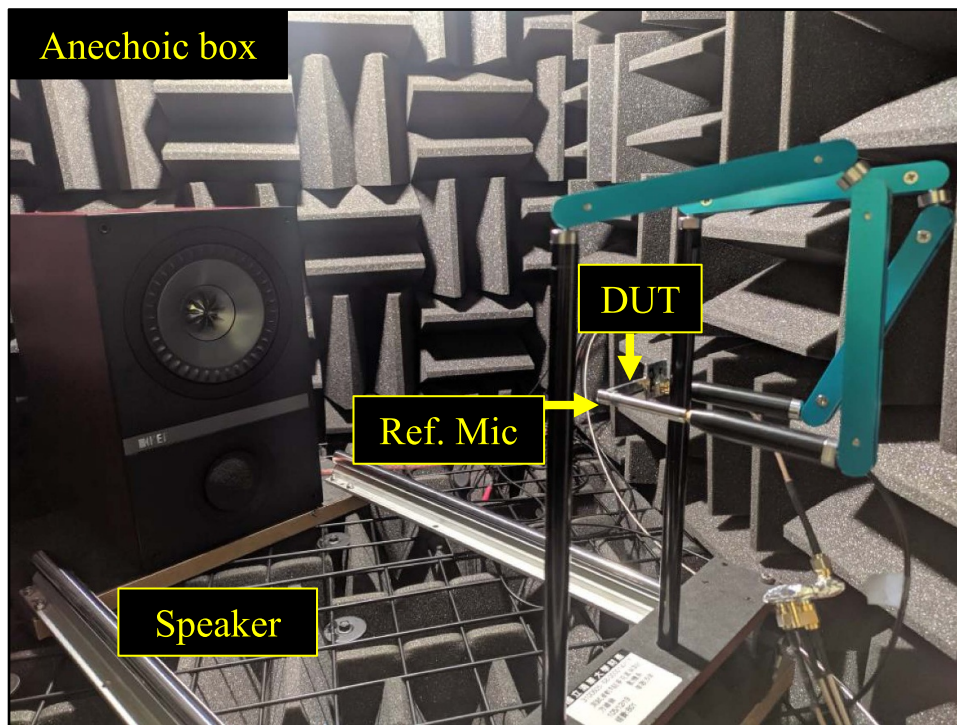


Figure 10. (a) The schematic illustration and (b) the photo, to show the acoustic measurement setup.

monitored by a commercial reference microphone (GRAS-46BE 1/4", GRAS Sound & Vibration A/S, Denmark). The output signal from the DUT is amplified by the circuits and then transmitted to the acoustic analyzer (IEA-EA2, IEA Electro-Acoustic Technology Co., Ltd, Taiwan) for data analysis. Figure 11(a) further shows the amplifying circuit composed of the two-stage amplifier and the buffer. The charge

amplifier (the first stage) converts the charge signal output from the piezoelectric microphone to voltage signal. The voltage amplifier (the second stage) ensures the flexibility and adjustability of overall circuit gain. Note the circuit has a low cut-off frequency $f = 1/2\pi R_f C_f$ determined by the feedback resistor (R_f) and the capacitor (C_f). Thus the feedback resistor and capacitor are designed to avoid affecting

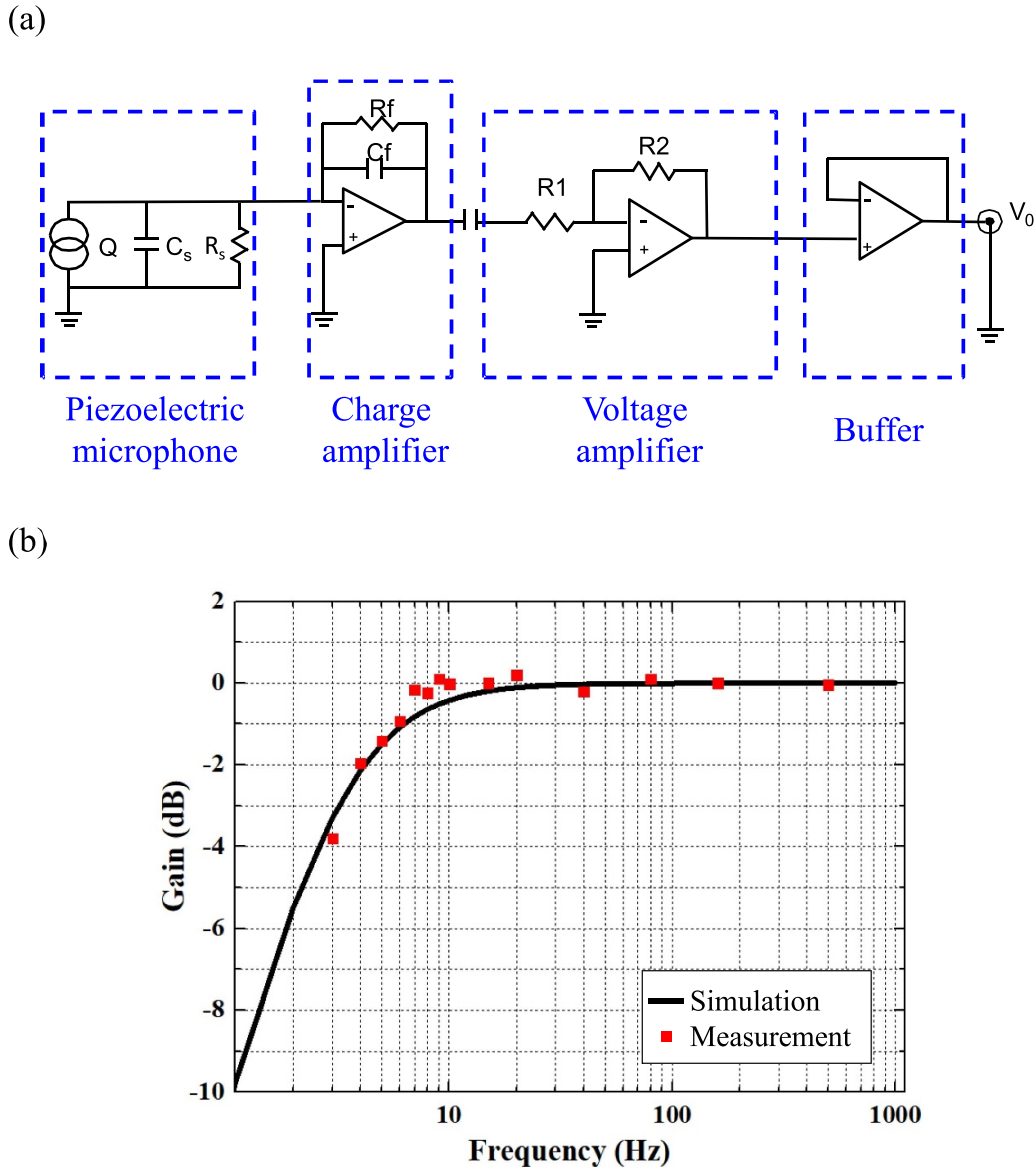


Figure 11. (a) The amplifying circuit design and (b) the measured frequency responses.

the bandwidth of microphone. Simulation and measurement results shown in figure 11(b) show the cutoff frequency of the circuit lies at 3.2 Hz, which is sufficiently lower than the operating bandwidth of microphone (20 Hz–20 kHz). Meaning that the circuit offers a uniform gain for the entire microphone bandwidth.

Figure 12 shows typical SNR measurement results (ref. 1 V/1 Pa) of the three different types of PZT/Si unimorph cantilever microphones at 1 kHz. The results indicate the sensitivity of the proposed design (rectangular Si cantilever with triangular PZT layer) at 1 kHz is -33.2 dBV, and the SNR is 82.4 dB. For the reference microphone design shown in figure 3(b) (rectangular Si cantilever fully covered with PZT film), the sensitivity is -35.2 dBV and the SNR is 77.9 dB. In addition, for the reference microphone design shown in figure 3(c) (triangular Si cantilever fully covered with PZT

film), the sensitivity becomes -38.6 dBV, and the SNR is 72.6 dB. Thus, as compared to the PZT/Si triangular cantilever microphone, the proposed design could enhance the SNR for up to 9.8 dB. Moreover, measurements also indicate the SNR enhancements are ranging 10.7–12.3 dB in the frequency range of 2–8 kHz. Note that the SNR of all designs has less than 2 dB variation from 1 kHz to 8 kHz. Measurements demonstrate the proposed design could increase the output electrical energy with the same sensing area. For the total harmonic distortion (THD) measurement, the THD of these three designs is less than 0.3% under the excitation conditions of 1 kHz and 1 Pa. Therefore, these three unimorph structure designs have no significant difference in THD.

It is worth to note that the cantilever structures of microphone will be bent by the residual stresses of thin films,

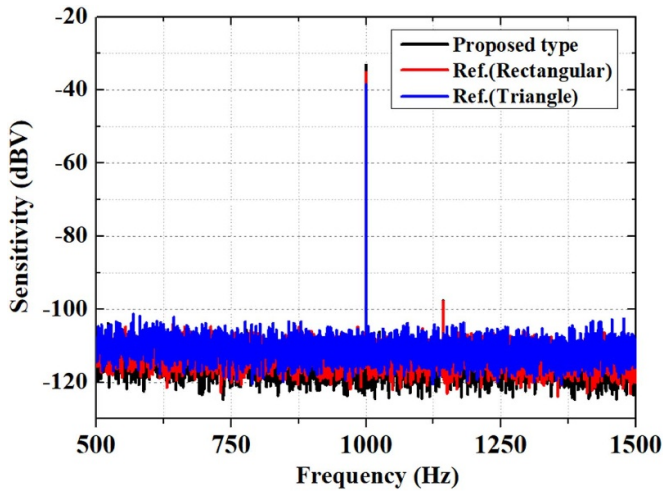


Figure 12. The measured SNRs respectively for the proposed and reference designs at 1 kHz.

and hence the gap between cantilever array will be enlarged. Since the gap size between cantilever array critically influences the sensitivity of the microphone at low frequency range [15], this is a design concern for the proposed microphone. The stiffness of the proposed PZT/Si cantilever design will be reduced after partially removing the PZT layer. Thus, as compare with the reference designs, the proposed cantilever has a larger bending deformation at the same thin film residual stresses. The tip deflections of cantilevers characterized by the white light interferometer are respectively 22.3 μm (for the proposed design), 16.2 μm (for the reference rectangular-cantilever design), and 5.6 μm (for the reference triangular-cantilever design). Moreover, measurements in figure 13 show the frequency responses of the proposed and reference designs. The low cutoff frequency respect to 1 kHz of the reference triangular-cantilever design, the reference rectangular-cantilever design, and the proposed design are 306 Hz, 335 Hz, and 411 Hz, respectively. It is possible to lower the cutoff frequency by reducing the thin film residual stresses or designing the pattern of PZT film for stiffness enhancement. In summary, the predicted and measured performances of the three different microphone designs are summarized in table 1.

5. Conclusions

The piezoelectric microphone has attracted attentions in recent years. Since no back plate and sensing gap are required, the air damping is not a design concern and the structure is less sensitive to the water and dust. Moreover, the piezoelectric microphone also offers the advantages of large dynamic range and low power consumption. However, the SNR of piezoelectric microphone still needs to be improved. This study presents the design, fabrication, and testing of a novel piezoelectric MEMS microphone for SNR enhancement. In this design, the unimorph cantilever array with the

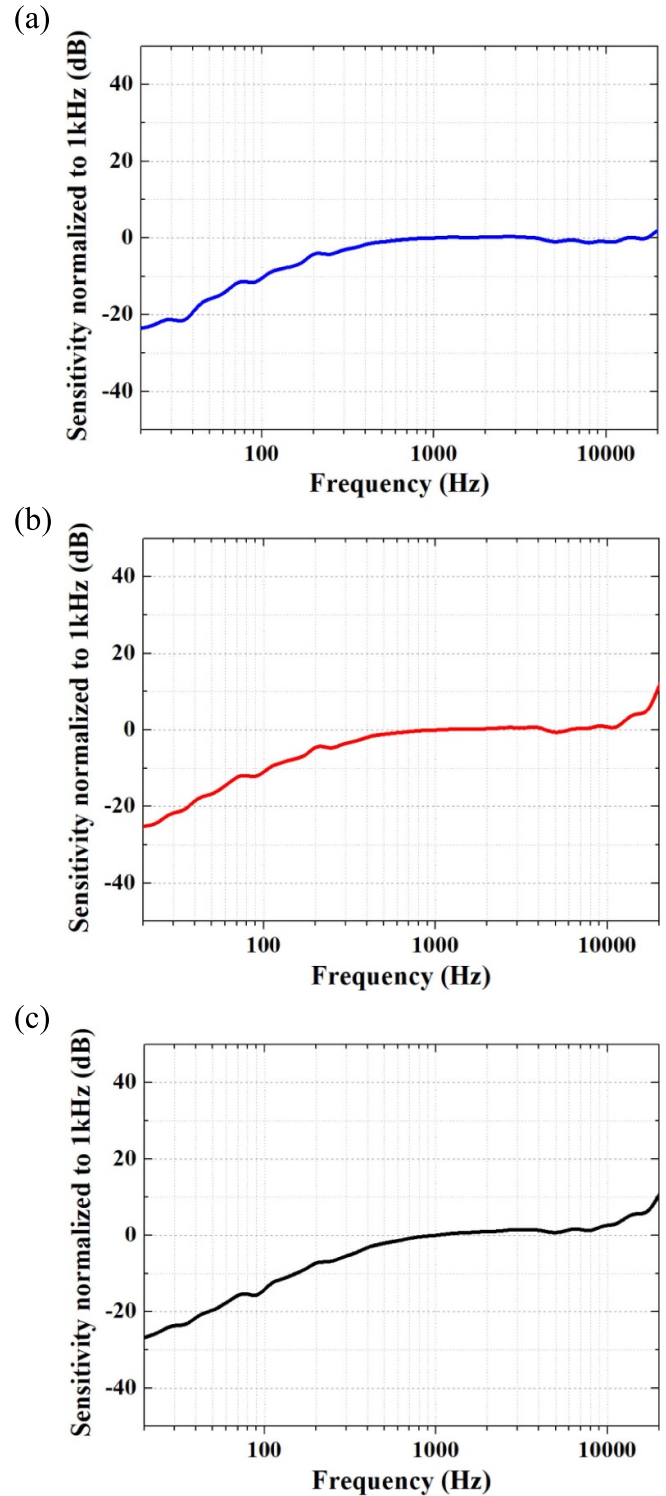
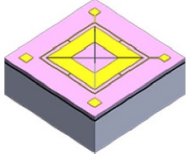
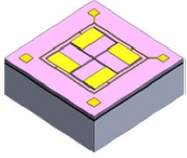
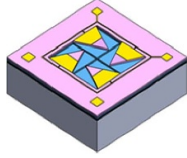


Figure 13. Measured frequency responses of, (a) the reference PZT/Si triangular cantilever, (b) the reference PZT/Si rectangular cantilever, and (c) the proposed Si rectangular cantilever with patterned PZT film.

patterned (triangular shape) PZT film on top of a rectangular Si layer is demonstrated. In comparison, the rectangular and triangular unimorph cantilever arrays with fully covered

Table 1. The predicted and measured performances of the three different microphone designs.

	Unit	Reference (triangle)	Reference (rectangular)	Proposed type	
					
Simulation	Average in-plane normal stress	kPa	3.7	10.4	13.0
	Output electrical energy (at 50% electrode)	aJ	1.14	6.03	7.09
	Output electrical energy (Maximum)	aJ	1.17	6.11	7.09
Measurement	SNR	dB	72.6	77.9	82.4
	Low cutoff frequency respect to 1 kHz	Hz	306	335	411

PZT film are also investigated. For fair comparison, the proposed and reference PZT microphone arrays in figures 7(a)–(c) have the same footprint of $800\ \mu\text{m} \times 800\ \mu\text{m}$. Simulations show the proposed design has the highest output electrical energy which indicates the proposed design could successfully enhance the SNR. Moreover, acoustic measurements in the standard anechoic box show the proposed Si cantilever with patterned PZT film design could significantly improve the SNR. As compared to the reference microphone with triangular PZT/Si unimorph cantilever, the proposed design shows a 9.8 dB enhancement in SNR. The stiffness of the proposed PZT/Si unimorph cantilever design will be reduced after partially removing the PZT layer. It is important to properly control the residual stresses of thin film to reduce the influence on low frequency responses for the proposed microphone.

Data availability statement

All data that support the findings of this study are included within the article (and any supplementary files).

Acknowledgments

This project was supported by the ministry of science and technology (MOST) of Taiwan under the Grant Nos. MOST 110-2218-E-007-032, MOST 109-2926-I-007-503, and MOST 109-2923-E-007-007. The authors would like to thank the Center of Nano Science and Technology at National Tsing Hua University, and Taiwan Semiconductor Research Institute for providing the fabrication facilities.

ORCID iD

Weileun Fang  <https://orcid.org/0000-0002-3309-0407>

References

- [1] Choi C, Kong D, Kim J and Bang S 2003 Speech enhancement and recognition using circular microphone array for service robots *Proc. IEEE/RSJ Int. Conf. on Intelligent Robots and Systems (Las Vegas, NV, USA)* vol 4 pp 3516–21
- [2] Jung Y-W, Lee J, Kong D, Kim J and Lee C 2003 High-quality speech acquisition and recognition system for home-agent robot *IEEE Int. Conf. on Consumer Electronics (Los Angeles, CA, USA)* pp 354–5
- [3] Loeppert P V and Lee S B 2006 SiSonic™ —the first commercialized MEMS microphone *Proc. Solid-State Sensors Actuators and Microsystems Workshop (Hilton Head Island, SC, June)* pp 27–30
- [4] Weigold J W, Brosnihan T J, Bergeron J and Zhang X 2006 A MEMS condenser microphone for consumer applications *IEEE MEMS Conf. (Istanbul, Turkey, 22–26 January)* pp 86–89
- [5] Lo S-C, Wang J-J, Wu M and Fang W 2017 Sensitivity improvement of no-back-plate MEMS microphone using polysilicon trench-refilled process *Transducers 2017 (Kaohsiung, Taiwan)* pp 1171–4
- [6] Lo S-C, Yeh S-K, Wang J-J, Wu M, Chen R and Fang W 2018 Bandwidth and SNR enhancement of MEMS microphone using two poly-Si micromachining process *IEEE MEMS Conf. (Belfast, UK, 21–25 January)* pp 1064–7
- [7] Dehé A, Wurzer M, Földner M and Krumbein U 2013 Design of a poly silicon MEMS microphone for high signal-to-noise ratio *2013 Proc. of the European Solid-State Device Research Conf. (Bucharest)* pp 292–5
- [8] Lo S-C, Chan C-K, Wu M and Fang W 2020 Design and implementation of differential MEMS microphones using the two polysilicon processes for SNR enhancement *J. Micromech. Microeng.* **30** 055006

- [9] Lee S S, Ried R P and White R M 1996 Piezoelectric cantilever microphone and microspeaker *J. Microelectromech. Syst.* **5** 238–42
- [10] Huang J-L, Lo S-C, Wang J-J, Lu C-E, Tseng S-H, Wu M-C and Fang W 2017 High sensitivity and high S/N microphone achieved by PZT film with central-circle electrode design *IEEE MEMS Conf. (Las Vegas, USA)* pp 1188–91
- [11] Williams M, Griffin B, Reagan T, Underbrink J and Sheplak M 2012 An AlN MEMS piezoelectric microphone for aeroacoustic applications *J. Microelectromech. Syst.* **21** 270–83
- [12] Baumgartel L, Vafanejad A, Chen S and Kim E 2013 Resonance-enhanced piezoelectric microphone array for broadband or prefiltered acoustic sensing *J. Microelectromech. Syst.* **22** 107–14
- [13] Kuntzman M and Hall N 2014 Sound source localization inspired by the ears of the *Ormia ochracea* *Appl. Phys. Lett.* **105** 033701
- [14] Zhang Y, Bauer R, Windmill J F C and Uttamchandani D 2016 Multi-band asymmetric piezoelectric MEMS microphone inspired by the *Ormia ochracea* *IEEE MEMS Conf. (Shanghai, China)* pp 1114–7
- [15] Littrell R J 2010 High performance piezoelectric MEMS microphones PhD Thesis The University of Michigan
- [16] Littrell R J and Grosh K 2012 Modeling and characterization of cantilever-based MEMS piezoelectric sensors and actuators *J. Microelectromech. Syst.* **21** 406–13
- [17] Littrell R J and Grosh K 2013 Noise minimization in micromachined piezoelectric microphones *J. Acoust. Soc. Am.* **133** 3359
- [18] Seo Y, Corona D and Hall N 2017 On the theoretical maximum achievable signal-to-noise ratio (SNR) of piezoelectric microphones *Sens. Actuators A* **264** 341–6
- [19] Ledermann N, Muralt P, Baborowski J, Forster M and Pellaux J 2004 Piezoelectric $\text{Pb}(\text{Zr}_x, \text{Ti}_{1-x})\text{O}_3$ thin film cantilever and bridge acoustic sensors for miniaturized photoacoustic gas detectors *J. Micromech. Microeng.* **14** 1650–8
- [20] Wang Q-M, Du X H, Xu B and Cross L 1999 Theoretical analysis of the sensor effect of cantilever piezoelectric benders *J. Appl. Phys.* **85** 1702–12
- [21] Zhang L, Ren T, Liu J, Liu L and Li Z 2002 Fabrication of a cantilever structure for piezoelectric microphone *Japan J. Appl. Phys.* **41** 7158–9
- [22] İlik B, Koyuncuoğlu A, Şardan-Sukas Ö and Külah H 2018 Thin film piezoelectric acoustic transducer for fully implantable cochlear implants *Sens. Actuators A* **280** 38–46
- [23] Lee S S and White R M 1998 Piezoelectric cantilever acoustic transducer *J. Microelectromech. Syst.* **8** 230–8
- [24] Tomimatsu Y, Takahashi H, Kobayash T, Matsumoto K, Shimoyama I, Itoh T and Maeda R 2013 A piezoelectric cantilever with a Helmholtz resonator as a sound pressure sensor *J. Micromech. Microeng.* **23** 114003
- [25] Chen Y-C, Lo S-C, Cheng H-H, Wu M, Huang I and Fang W 2019 Design of cantilever diaphragm array piezoelectric MEMS microphone for signal-to-noise ratio enhancement *IEEE Sensors Conf. (Montreal, QC, Canada)* pp 1–4
- [26] Beer F P, Johnston E R, Eisenberg E R and Sarubbi R G 2001 *Vector Mechanics for Engineers. Statics and Dynamics* 9th edn (New York: McGraw-Hill)
- [27] Grosh K and Littrell R J 2019 Acoustic transducer with gap-controlling geometry and method of manufacturing an acoustic transducer United States Patent No. 10,284,960
- [28] Cheng H-H, Lo S-C, Huang Z-R, Wang Y-J, Wu M and Fang W 2020 On the design of piezoelectric MEMS microspeaker for the sound pressure level enhancement *Sens. Actuators A* **306** 111960
- [29] Dekkers M, Boschker H, van Zalk M, Nguyen M, Nazeer H, Houwman E and Rijnders G 2012 The significance of the piezoelectric coefficient $d_{31,\text{eff}}$ determined from cantilever structures *J. Micromech. Microeng.* **23** 025008